Desorption and sublimation kinetics for fluorinated aluminum nitride surfaces

Cite as: J. Vac. Sci. Technol. A **32**, 051402 (2014); https://doi.org/10.1116/1.4891650
Submitted: 08 July 2014 • Accepted: 18 July 2014 • Published Online: 31 July 2014

Sean W. King, Robert F. Davis and Robert J. Nemanich

Desorption and sublimation kinetics for fluorinated aluminum nitride surfaces

Sean W. King[a] and Robert F. Davis[b]
Department of Materials Science and Engineering, North Carolina State University, Raleigh, North Carolina 27695

Robert J. Nemanich[c]
Department of Physics, North Carolina State University, Raleigh, North Carolina 27695

(Received 8 July 2014; accepted 18 July 2014; published 31 July 2014)

The adsorption and desorption of halogen and other gaseous species from surfaces is a key fundamental process for both wet chemical and dry plasma etch and clean processes utilized in nanoelectronic fabrication processes. Therefore, to increase the fundamental understanding of these processes with regard to aluminum nitride (AlN) surfaces, temperature programmed desorption (TPD) and x-ray photoelectron spectroscopy (XPS) have been utilized to investigate the desorption kinetics of water (H_2O), fluorine (F_2), hydrogen (H_2), hydrogen fluoride (HF), and other related species from aluminum nitride thin film surfaces treated with an aqueous solution of buffered hydrogen fluoride (BHF) diluted in methanol (CH_3OH). Pre-TPD XPS measurements of the CH_3OH:BHF treated AlN surfaces showed the presence of a variety of Al-F, N-F, Al-O, Al-OH, C-H, and C-O surfaces species in addition to Al-N bonding from the AlN thin film. The primary species observed desorbing from these same surfaces during TPD measurements included H_2, H_2O, HF, F_2, and CH_3OH with some evidence for nitrogen (N_2) and ammonia (NH_3) desorption as well. For H_2O, two desorption peaks with second order kinetics were observed at 195 and 460 °C with activation energies (E_d) of 51 ± 3 and 87 ± 5 kJ/mol, respectively. Desorption of HF similarly exhibited second order kinetics with a peak temperature of 475 °C and E_d of 110 ± 5 kJ/mol. The TPD spectra for F_2 exhibited two peaks at 485 and 585 °C with second order kinetics and E_d of 62 ± 3 and 270 ± 10 kJ/mol, respectively. These values are in excellent agreement with previous E_d measurements for desorption of H_2O from SiO_2 and AlF_x from AlN surfaces, respectively. The F_2 desorption is therefore attributed to fragmentation of AlF_x species in the mass spectrometer ionizer. H_2 desorption exhibited an additional high temperature peak at 910 °C with $E_d = 370 \pm 10$ kJ/mol that is consistent with both the dehydrogenation of surface AlOH species and H_2 assisted sublimation of AlN. Similarly, N_2 exhibited a similar higher temperature desorption peak with $E_d = 535 \pm 40$ kJ/mol that is consistent with the activation energy for direct sublimation of AlN. © *2014 American Vacuum Society*. [http://dx.doi.org/10.1116/1.4891650]

I. INTRODUCTION

The success of the micro, now modern day nanoelectronics industry,[1,2] has largely been enabled by the ability of various different aqueous[3–5] and dry[6–8] halogen based etch chemistries[9–11] to remove oxide, metal, and organic surface contaminants,[12–14] and transfer optical lithography generated photoresist patterns into a substrate or thin film material.[15] At a fundamental level, these processes all rely on the adsorption, desorption, and transport away of various reactive and by-product species from the target etch surface[16–18] (as well as more complex ion and electron/charged species-surface interactions for dry plasma based processes[19–22]). Accordingly, numerous studies have been reported in the scientific literature focusing on the surface processes involved in both aqueous and dry plasma etch chemistries such as HF wet etching of Si and SiO_2,[23,24] HCl wet etching of GaAs,[25] HCl/Cl_2 plasma etching of Al,[26–31] Si,[32–34] and GaAs,[34–36] and F_2/CF_4 plasma etching of Si,[37–41] SiO_2,[39–44] and Si_3N_4.[45–48] These studies have focused mainly on the interaction between the etch chemistry and the surface of the targeted etch material and associated photoresist,[48] hard mask,[49] and etch stopping[47] materials, or the sidewall polymer materials intentionally deposited during the etch process to facilitate etching of high aspect ratio features.[50–54] Less characterized has been the interactions between various plasma etch chemistries and the exposed surfaces of materials comprising the internal etch chamber hardware.[55–58] The corrosion of internal chamber hardware surfaces by the etch chemistry is particularly important as it can lead to a variety of technical problems including process drift,[59–63] first wafer effects,[63] particle/yield excursions,[59–66] eventual part failure,[67,68] and diminished tool availability.[59–62,66]

For the above reasons, we have chosen to investigate the desorption kinetics of H_2O, HF, F_2, and other species from AlN surfaces. The desorption of these species from AlN

[a]Present address: Logic Technology Development, Intel Corporation, Hillsboro, OR 97124; electronic mail: sean.king@intel.com
[b]Present address: Department of Materials Science and Engineering, Carnegie Mellon University, Pittsburgh, PA 15260.
[c]Present address: Department of Physics, Arizona State University, Tempe, AZ 85287.

surfaces is important relative to the above technical challenges for a number of reasons. First, H_2O and surface hydroxides (−OH) are prevalent on all practical ambient exposed surfaces,[69,70] and H_2O is a component in most aqueous based etching, cleaning, and rinsing processes for Al, Al_2O_3, and AlN surfaces.[71–76] The degassing and thermal desorption of moisture prior to or during processing is also important to the technical success of many processes,[77–86] and can be a significant device performance or reliability concern.[87–94]

Similarly, HF based wet chemistries are commonly utilized for reducing surface oxides on AlN, Al_2O_3, and other Al containing surfaces,[73,74] and in some cases fluorine is utilized in plasma etch chemistries for AlGaN alloys.[95] In contrast, AlN and Al_2O_3 are also commonly utilized as etch stopping materials for various fluorine and fluorocarbon based wet and dry plasma etch chemistries.[96–98] Lastly, anodized aluminum, AlN, and Al_2O_3 are typically used for the manufacture of the internal chamber hardware of many semiconductor plasma etch and deposition systems.[99,100] The selection of aluminum based materials for these last two applications is in many cases due to an extreme resistance of aluminum based materials to etching by fluorine based etch chemistries. This resistance is primarily a result of the formation of a low volatility AlF_x or AlF_3 surface layer that passivates the surface and largely prevents further corrosion.[101,102] For chamber hardware applications though, this AlF_3 passivation layer can continue to slowly grow in thickness causing a gradual change in process chamber impedance and eventually crack and flake off leading to particulate formation and yield excursions.[59–62] The nature of how such AlF_x/AlF_3 layers form and grow is directly related to the kinetics of fluorine desorption from Al and AlF_3 surfaces. Therefore, knowledge of the kinetics of moisture and fluorine desorption from AlN surfaces should greatly aid modeling of Al containing surfaces in aqueous and fluorine based semiconductor, ceramic, and other process chemistries.

Prior investigations of the thermal desorption of fluorine from Al containing surfaces have been fairly limited and in some cases convoluted with other exposed surfaces.[103–109] For example, Aoki *et al.* investigated the desorption of AlF and other etch by-products from deep-submicron contact holes CF_4 plasma etched into SiO_2 with Al metal exposed at the bottom of the via.[103] For such surfaces, temperature programmed desorption (TPD) measurements showed the desorption of H_2 and a range of CF_x, AlF_x, and $AlCH_x$ related species with peak intensities occurring at $T_{max} = 500 \pm 30\,^{\circ}C$. Similar TPD studies by Yu *et al.* of Al surfaces exposed to WF_6 observed the desorption of AlF^+ and AlF_2^+ species with peak intensities occurring at ~470 °C.[104] Based on the relative intensity of the species detected and how T_{max} changed with F surface coverage, Yu *et al.* concluded that AlF_2 was the primary desorbing specie and that the desorption kinetics were likely second order. More detailed molecular beam mass spectrometry (MBMS) investigations by Watanabe *et al.* of AlN thermally etched by XeF_2 found that N_2 and AlF_3 were the primary etch and desorption products with AlF_3 desorption beginning at temperatures of ~500 °C and N_2 at 623 °C.[106,107] Watanabe *et al.* additionally investigated the thermal desorption behavior of a 5 μm thick AlF_3 film grown on Al_2O_3 in a 15% HF solution and found that below 350 °C, F was the primary desorption specie, but at higher temperatures, AlF_2 became the dominant desorbing specie.[108] From a detailed analysis of their studies, they deduced activation energies for AlF_3 and AlF_2 desorption of 1.1 ± 0.03 eV (106 kJ/mol) and 2.8 ± 0.04 eV (270 kJ/mol), respectively (see Table I).

TABLE I. Summary of reported temperatures and kinetic parameters for desorption of various species from AlN and other relevant surfaces.

Desorbing Specie	Surface	Temperature (°C)	Order (1st, 2nd)	E_d (kJ/mol)	ν_d	Reference
H_2O	Al_2O_3 $(11\bar{2}0)$	337	2nd	61.9 ± 4	$3 \pm 1 \times 10^5$ ML^{-1} s^{-1}	116
H_2O	Al_2O_3 (0001)	100–250	1st	96–171	—	117
H_2O	SiO_2	192	1st	23 ± 2	5.1 s^{-1}	84
H_2O	SiO_2	355	1st	55 ± 17	6.0×10^2 s^{-1}	84
H_2O	SiO_2	490	1st	89 ± 1	2.5×10^4 s^{-1}	84
H_2O	SiO_2	631	1st	202 ± 18	1.4×10^{10} s^{-1}	84
H_2O	SiO_2	400–500		79.5	—	82
NH_3	GaN	350–780	1st	220–260	10^{13} s^{-1}	142
NH_3	AlN $(000\bar{1})$	—	—	240	—	144
C_xH_y	AlN/Al_2O_3 (0001)	375	1st	182	10^{13} s^{-1}	142
CO	AlN/Al_2O_3 (0001)	304	1st	162	10^{13} s^{-1}	142
O_2	AlN/Al_2O_3 (0001)	1017	1st	370	10^{13} s^{-1}	142
H_2	AlN/GaN (0001)	—	2nd	230	0.01 cm^2/s	73
AlF_x	AlN	523	—	106 ± 3	—	106
AlF_2	AlN	523	—	270 ± 4	—	106
AlN	AlN	1040	1st	414	10^{13} s^{-1}	142
AlN	AlN (0001)	1100	—	399	—	145
AlN	AlN $(000\bar{1})$	1100	—	450	—	145
Al/AlN	AlN (0001)	1300	1st	520 ± 30	—	146
AlH	AlN (0001)	—	1st	456	—	142

Concerning H_2O desorption from AlN, the authors are aware of only a single TPD study by Saito *et al.*,[110] which showed peak H_2O desorption from AlN powders occurred at ~50 °C. However, more detailed studies of the desorption of H_2O from other Al containing surfaces such as oxidized Al, Al_2O_3, and AlAs have been reported.[110–119] For ice layers condensed on oxidized Al (100) surfaces, zeroth order desorption of H_2O was observed by Memmert *et al.* at approximately −173 °C followed by H_2 desorption at 197–223 °C (presumably the result of decomposition of surface −OH groups).[113] Similar results were also observed by Polzl for condensed H_2O desorption from oxidized Al (111) surfaces where peaks in both H_2O and H_2 desorption were observed at 47 and 377 °C and attributed to the decomposition and recombination of different surface aluminum hydroxide species.[114] For nonpolar Al_2O_3 $(11\bar{2}0)$ surfaces, Schildbach observed the peak in H_2O desorption to occur at 337 °C for a low coverage of 0.1 monolayer (ML) and gradually decrease to 177 °C for a coverage as high as 0.42 ML.[115] For a coverage of several monolayers (5–10 ML), a second desorption peak at approximately 57 °C was observed. H_2 and OH desorption signals were attributed to cracking of H_2O by the mass spectrometer ionizer. For the low coverage H_2O desorption peak (0.07–0.25 ML), they determined second order desorption kinetics with an activation energy of 61.9 ± 4 kJ/mol and pre-exponential of $3 \pm 1 \times 10^5$ ML^{-1} s^{-1} (see Table I). For Al_2O_3 (0001) surfaces, Nelson *et al.*[117] and Elam *et al.*[118] observed a broad H_2O desorption peak with a maximum at 102 °C. The position of this peak increased significantly up to 252 °C by pre-annealing the Al_2O_3 sample at 202 °C prior to performing the TPD measurement.[118] Based on these results, Nelson *et al.* concluded that the H_2O desorption kinetics were dictated solely by the hydroxyl surface coverage and exhibited a range of different desorption activation energies. Based on the observation that the surface hydroxyl groups have limited mobility, the authors estimated the activation energy for desorption to be 96–171 kJ/mol for first order kinetics (and assuming a pre-exponential $(\nu) = 10^{13}$/s). Lastly, Mitchell observed similar behavior for desorption of H_2O from AlAs (100) surfaces where desorption was observed to occur at 277–302 °C and attributed to recombinative desorption from surface aluminum hydoxides.[119]

To gain a better understanding of the desorption kinetics of F_2, HF, and H_2O from practical AlN surfaces, we have performed a detailed kinetic analysis of TPD spectra obtained from polycrystalline reactively sputtered AlN thin films chemically treated in a 1:1 methanol (MeOH):buffered HF (BHF) solution. In a previous report, we have shown that H_2O desorption is observed to occur at both 195 and 460 °C, whereas HF and F_2 desorption occur primarily at 530° and 585°, respectively. In this study, we report the activation energy for desorption of these and other species from AlN surfaces based on a detailed kinetic analysis of the TPD spectra. We find that the desorption activation energies determined for H_2O, HF, and F_2 are in agreement with some of the previously mentioned studies of H_2O and AlF_x desorption from related Al, AlN, and Al_2O_3 surfaces. Detailed analysis of TPD spectra for H_2 and N_2 also provided insight into the desorption kinetics of NH_3 from AlN, and the kinetics and mechanisms for AlN sublimation at temperatures >900 °C.

II. EXPERIMENT

The substrates and the sample preparation procedures used in these experiments have been described in detail elsewhere;[120–122] however, a brief overview is presented herein. The polycrystalline AlN sample utilized in this investigation was prepared via reactive ion sputtering onto a 1 in. diameter Si (111) wafer.[73] The AlN surface was fluorinated by dipping in a 1:1 MeOH (CH_3OH):BHF (7:1 NH_4F:HF) solution for 5 min and then immediately loading into a vacuum loadlock.[123] The temperature programmed desorption measurements were performed in an ultrahigh vacuum (UHV) gas-source molecular beam epitaxy (GSMBE) system designed for the growth of AlN and GaN thin films and attached to the vacuum load lock via a UHV transfer line.[124] The GSMBE was additionally equipped with a Hiden Analytical 0–200 amu quadrapole mass spectrometer (QMS) fitted inside a differentially pumped chamber having a 0.5 cm diameter opening.[121] For TPD measurements, the sample holder/heater was positioned <1 cm from the front of the QMS opening.

The TPD experiments were conducted to a maximum temperature of ~1000 °C using a heating rate of 20–60 °C/min generated by a W filament heater positioned behind the AlN/Si sample.[125] During each TPD measurement, the QMS monitored m/e^- 2, 12, 14, 16, 18, 19, 20, 28, 29, 31, 32, and 38. These m/e^- ratios were selected based on both data acquisition limitations and a prior TPD study by Pietsch *et al.*[77] of HF and NH_4F processed Si (111) wafers that identified these m/e^- ratios as representing the primary species desorbing from the Si surface such as: H_2, H_2O, HF, N_2, CO, CH_3OH, CF_x, O_2, and F_2. Desorption of Al containing species in the TPD measurements were not investigated due to signal to noise versus sampling rate considerations, and a desire to focus on the desorption of lower m/e^- ratio species not investigated in detail in prior investigations of fluorinated Al, Al_2O_3, and AlN surfaces.[103–109]

To calibrate the hydrogen desorption signal from the fluorinated AlN surfaces, hydrogen desorption from a Si (111)–(7 × 7) surface exposed to a saturation dose of atomic hydrogen from a hot rhenium filament inside the GSMBE was also examined.[126] The saturation surface coverage of hydrogen from a Si (111) surface has been previously determined to be 1.25 monolayer ($ML = 7.8 \times 10^{14}/cm^2$) by Culbertson *et al.*[127] By equilibrating the area under the H_2 TPD spectra from a saturated Si(111) surface to $8.75 \times 10^{14}/cm^2$, we were able to calibrate against a known standard the intensity of the hydrogen desorption from our AlN surfaces and estimate the coverage of other species assuming similar sensitivity.

To ensure that all the desorbed species originated only from the substrate and not from other surfaces (e.g., sample heater), TPD measurements were also performed on clean and thoroughly degassed Si wafers prior to each MeOH:BHF-AlN TPD measurement. In these experiments, none of the desorption features observed in the MeOH:BHF-

AlN TPD measurements were noticed. Detection of species desorbing from the molybdenum sample holder was minimized by the designed geometry of the experiment. Specifically, line of sight desorption of species from the molybdenum sample holder into the QMS was greatly minimized by the large diameter of the AlN/Si sample (2.54 cm) and the significantly smaller QMS chamber opening (0.5 cm).[126]

Additional spurious effects may also occur in TPD experiments such as electron stimulated desorption (ESD) of H or F caused by electrons from the mass spectrometer ionizer.[128,129] While enclosing the mass spectrometer in the differentially pumped chamber may help to minimize this effect, we were not able to independently bias the chamber opening to completely eliminate this effect. Thus, some ESD effects may be present in our data. However, we feel this effect would only contribute to our background H_2 signal and not significantly alter our conclusions.

Kinetic treatments of TPD spectra normally use the Polanyi–Wigner desorption rate (DR) equation[130,131]

$$-d\theta/dt = \mathrm{DR} = \nu_d \theta^n \exp\left(-E_d/RT\right), \quad (1)$$

where θ = surface coverage, ν_d = desorption jump frequency/pre-exponential, n = rate order, and E_d = desorption activation energy. In principal, ν_d, n, and E_d can all be dependent on θ; however, most analyses assume these parameters to be independent of θ. Using the latter approach and taking the logarithm of both sides of the above equation accompanied by mathematical rearrangement, one obtains

$$\ln\left(\mathrm{DR}\right) - n\ln\theta = \ln\nu_d - E_d/RT, \quad (2)$$

where if the correct rate order (n) is chosen, a plot of (ln (DR) − nlnθ) versus (1/T) yields a straight line and has a slope of $-E_d/R$ and a y-intercept of lnν_d. The mathematical methods used for analyzing (ln (DR) − nlnθ) versus (1/T) were identical to those of Parker *et al.*[131] Once n, ν, and E_d were determined from the above analysis, fits to the experimental data were generated by simply plotting $d\theta/dt$ using the Polanyi–Wigner equation and the extracted kinetic parameters.

In-situ x-ray photoelectron spectroscopy (XPS) spectra were collected before and after each TPD measurement using a separate vacuum system attached to the GSMBE via the UHV transfer line. The XPS spectra were collected using Al Kα radiation (hν = 1486.6 eV) and a 100 mm hemispherical electron energy analyzer (VG CLAM II).[132,133] A combined Gaussian–Lorentzian curve shape with a linear background was found to best represent the data. The XPS spectra were corrected for charging by adjusting the C 1s to 285.8 eV. This value was selected based on prior XPS measurements of similar HF treated 2 nm AlN epilayers grown on 6H-SiC (0001) where significant charging was not observed.[73,74]

III. RESULTS AND DISCUSSION

A. XPS and TPD

Figures 1–5 show representative XPS spectra of the F 1s, O 1s, C 1s, N 1s, and Al 2p core levels from MeOH:BHF

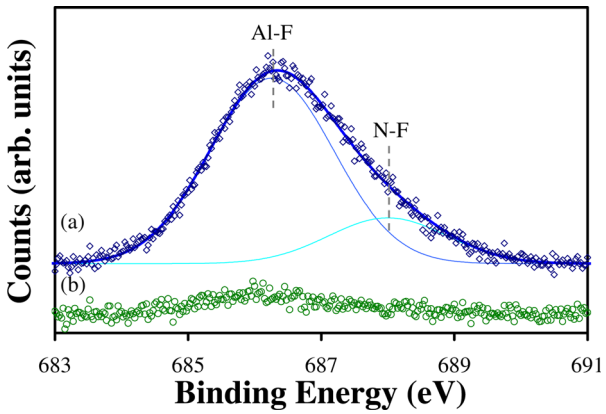

FIG. 1. (Color online) XPS spectrum of F 1s from MeOH:BHF treated AlN surface (a) before TPD and (b) after TPD.

treated AlN surfaces before and after TPD measurements. As shown in Fig. 1(a), a significant amount of fluorine is observed on the AlN surface post the MeOH:BHF surface treatment and loading into vacuum. We have previously shown that the F 1s spectra can be deconvoluted into two separate components at 686.3 and 688.0 eV attributable to Al-F and N-F bonding, respectively.[73] The latter assignment was supported by analysis of the N 1s core level [see Fig. 4(a)], which revealed a primary peak centered at 398.0 eV attributable to Al-N bonding and a small shoulder peak centered at ~399.9 eV attributable to surface N-F bonding.[73] Similarly, analysis of the Al 2p core level identified a primary peak at 74.8 eV attributable to Al-N bonding and a small shoulder peak at ~76.5 eV. The latter can be attributed to either Al-F or Al-O bonding. XPS measurements of Al surfaces exposed to WF_6 by Yu *et al.* have identified chemically shifted Al 2p peaks at 75.5 and 77.5 eV that were attributed to AlF_x and AlF_3, respectively.[104] Similarly, the Al 2p core level is generally located at 75–76 eV in Al_2O_3 and related amorphous aluminum oxide materials.[134]

As shown in Figs. 2(a) and 3(a), a significant amount of oxygen and carbon contamination was also observed on the AlN surface post MeOH:BHF treatment (as expected for the ambient processing). As shown previously, the O 1s could be deconvoluted into two peaks at 530.5 and 532.6 eV that

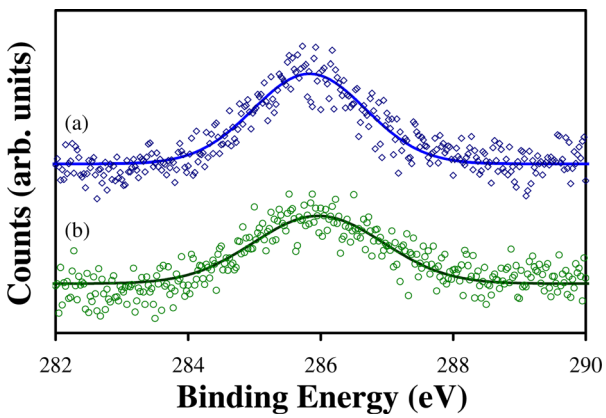

FIG. 2. (Color online) XPS spectrum of C 1s from MeOH:BHF treated AlN surface (a) before TPD and (b) after TPD.

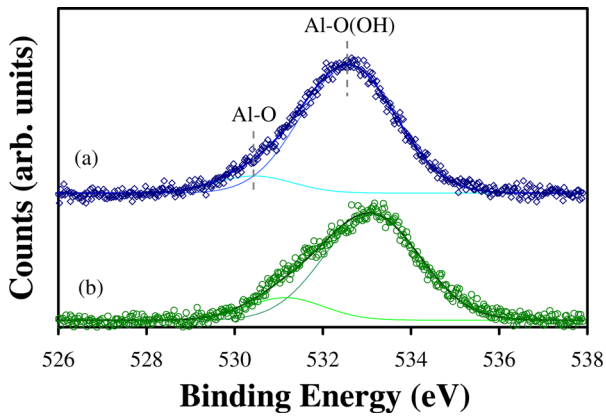

FIG. 3. (Color online) XPS spectrum of O 1s from MeOH:BHF treated AlN surface (a) before TPD and (b) after TPD.

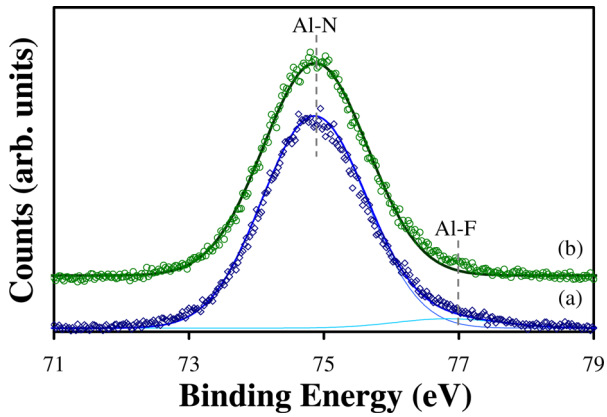

FIG. 5. (Color online) XPS spectrum of Al 2p from MeOH:BHF treated AlN surface (a) before TPD and (b) after TPD.

were attributed to Al-O and AlO(OH) bonding at the AlN surface.[73,74] Due to charge correction, the C 1s was intentionally centered at 285.8 eV and attributed to carbon contaminants containing C-O bonding. This assignment is consistent with the wet chemical processing of the AlN surface in a MeOH (CH_3OH) solution.[73]

Figures 6–10 show TPD spectra collected from the AlN surfaces for the various m/e^- ratios monitored. The strongest desorption signals were observed at m/e^- 2, 16, 18, 19, 20, and 28. The QMS signals at m/e^- 18, 19, and 20 were attributed directly to H_2O, F, and HF, respectively. As will be discussed later, m/e^- 28 could be attributed directly to either CO, N_2, or CO^+ produced by the fragmentation of desorbing CO_2 in the QMS ionizer.[135] Similarly, m/e^- 16 could be due to CH_4, or O^+ and $NH_2{}^+$ species created by QMS ionizer fragmentation of larger O and N containing species desorbing from the AlN surface (such as CO, CO_2, and NH_3).[135] The QMS intensities for species desorbing with $m/e^- = 12$, 14, 29, 31, 32, and 38 were observed to be a relative order of magnitude or more lower. The QMS signals at m/e^- 12 and 14 were attributed to C^+ and N^+ fragmentation species produced in the QMS ionizer from other desorbing entities. The QMS signal at m/e^- 29, 31, and 32 were attributed to desorption of CH_3OH. This was based on both the reported ionizer fragmentation pattern for CH_3OH[135] and the CH_3OH:BHF processing the AlN surface received. However, we do note that m/e^- 29 could, alternatively, be attributed to CO or N_2, m/e^- 31 to CF, and m/e^- 32 to O_2. The m/e^- 38 QMS signal was attributed to F_2 produced either due to direct desorption of F_2 or produced by QMS ionizer fragmentation of larger F containing species such as AlF_3 or NF_3.

As shown in Fig. 6, m/e^- 18 (H_2O) exhibited two desorption peaks at 195 and 460 °C, and starting at 800 °C an exponential increase in intensity to the maximum temperature investigated. This behavior is somewhat similar to that observed for H_2O desorption from oxidized Al and Al_2O_3 surfaces. As mentioned earlier, UHV studies have observed H_2O desorption to occur from oxidized Al and Al_2O_3 surfaces at temperatures of 180–380 °C. In addition, TPD studies by Shirai of the dehydration of Al_2O_3 powders have shown a series of H_2O desorption peaks at 250, 325, 405, 570, and 700 °C that are qualitatively in agreement with the observed H_2O desorption spectrum in Fig. 6 (and the H_2 spectrum in Fig. 10 to be discussed later).[136] In the Shirai study, the authors attributed the 250 °C peak to the desorption of hydrogen bonded H_2O (i.e., physisorbed H_2O) and the 325, 405, 570, and 700 °C peaks to recombinative desorption of H_2O from $Al(OH)_3$, AlOOH, associated OH, and isolated

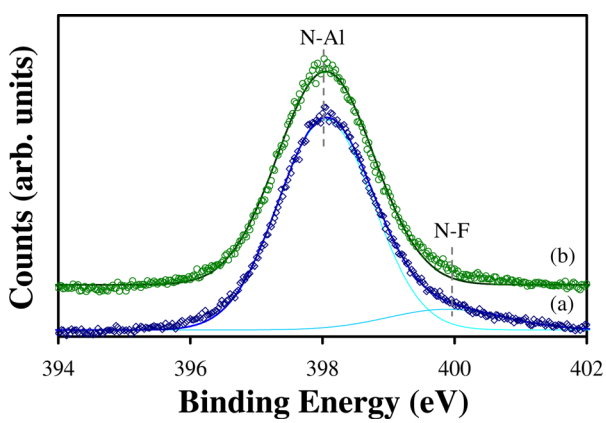

FIG. 4. (Color online) XPS spectrum of N 1s from MeOH:BHF treated AlN surface (a) before TPD and (b) after TPD.

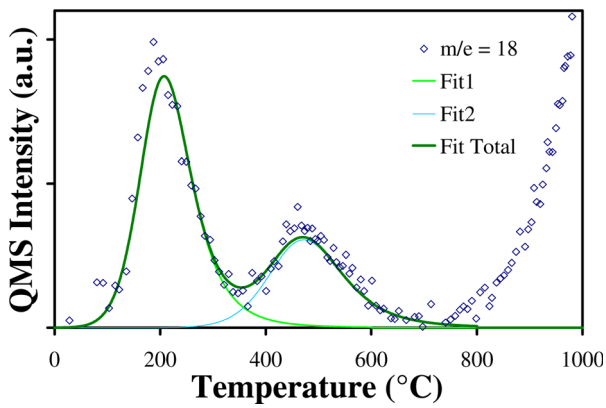

FIG. 6. (Color online) TPD spectrum from MeOH:BHF treated AlN surface for m/e^- 18. Diamonds represent experimental data and lines fits to the experimental data derived using the described kinetic analysis.

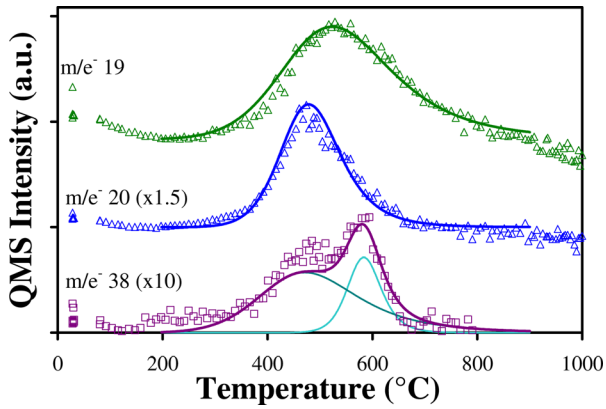

FIG. 7. (Color online) TPD spectrum from MeOH:BHF treated AlN surface for m/e$^-$ 19, 20, and 38. Symbols represent experimental data and lines fits to the experimental data derived using the described kinetic analysis.

OH groups, respectively. A similar pattern has also been observed for H_2O desorption and the dehydration of various spin-coated organosilica, plasma deposited, and thermally grown SiO_2 films[78–86,137,138] and Si (100) and (111) surfaces.[77,139] Specifically, Proost *et al.* has identified four different H_2O desorption peaks occurring at 190, 355, 490, and 630 °C that were attributed to desorption from physisorbed H_2O, tightly hydrogen bonded H_2O (i.e., chemisorbed H_2O), hydrogen bonded silanols (SiOH), and isolated silanols.[84,86]

Based on these prior observations of H_2O desorption from Al_2O_3 and SiO_2 surfaces, we attribute the observed H_2O desorption peak at 190 °C to desorption of hydrogen bonded/physisorbed water and the peak at 460 °C to hydrogen desorption from hydrogen bonded AlOH groups. We note that this assignment is consistent with the post TPD XPS measurements where a decrease in the total O 1s intensity was observed and more specifically a decrease in intensity for the higher binding energy ~532.5 eV component of the O 1s attributed to AlOH bonding [see Fig. 2(b)]. The H_2O desorption peak at 460 °C is also consistent with a prior combined XPS and thermal annealing study of fluorinated AlN surfaces where a decrease in O 1s intensity was observed after annealing from 400 to 600 °C.[73] The exponential tail starting at 800 °C could be due to H_2O desorption from isolated or subsurface OH groups, or an exponential increase in the background H_2O pressure in the GSMBE due to H_2O desorption from the sample heater or internal surfaces of the chamber heated by radiation from the sample and heater. The latter is consistent with the previously mentioned more detailed XPS thermal annealing measurements where an increase in O 1s intensity was observed after annealing at 950 °C and attributed to reaction of the AlN surface with background H_2O desorbing from the sample holder/heater and chamber walls.[73]

Figure 7 displays TPD spectra for m/e$^-$ 19 (F), 20 (HF), and 38 (F_2). The TPD spectrum for m/e$^-$ 20 (HF) exhibited a single sharp peak at 475 °C, whereas m/e$^-$ 19 (F) exhibited a much broader desorption peak spanning from 300 to 800 °C and centered at a slightly higher temperature of 530 °C. Although weaker in intensity, the TPD spectrum for m/e$^-$ 38 (F_2) exhibited two peaks at 485 and 585 °C. These results are consistent with the post TPD XPS measurements. As shown in Fig. 1(b), the intensity of the F 1s post TPD was reduced almost to below the detection level consistent with the observed desorption of HF and F_2 in Fig. 10. Likewise, the broad tail observed at higher binding energies in the pre-TPD N 1s spectra and attributed to N-F bonding also disappeared post TPD [see Fig. 4(b)]. The small shoulder peak on the Al 2p core level at 76.5 eV attributed to either Al-O or Al-F bonding was similarly barely detectable after the TPD measurements suggesting its relation to Al-F bonding [see Fig. 5(b)].

The broad nature of the m/e$^-$ 19 TPD peak is consistent with our prior combined XPS and thermal annealing study of fluorinated AlN surfaces where a gradual reduction in total F 1s intensity was observed after annealing from 400 to 1000 °C,[73] and could therefore be due to F produced by fragmentation of HF, F_2, or other F containing desorbing species in the QMS ionizer such as AlF_3 or NF_3. Desorption of AlF_3 is definitely consistent with the previously mentioned TPD and MBMS studies of fluorinated Al, AlN, and Al_2O_3 surfaces where peak desorption of AlF_x species was observed to occur at temperatures of 450–600 °C.[103–108] This also strongly correlates with the peaks in HF and F_2 desorption observed here at 480 and 585 °C and further suggests that at least a portion of the TPD spectra for m/e$^-$ 19, 20, and 38 may be due to ionizer fragmentation of AlF_x species not monitored. However, our prior combined thermal annealing and XPS measurements also support NF_x desorption in the same 400–600 °C window where a strong reduction in the F 1s intensity attributed to N-F bonding at 688.5 eV was observed in addition to a smaller reduction in Al-F bonding intensity at 686.5 eV.[73] Support for a more definitive assignment of these desorption features will be provided in Sec. III B covering the kinetic analysis of the TPD spectra.

Figure 8 shows the TPD spectra for m/e$^-$ 29, 31, and 32. Similar to m/e$^-$ 18, these spectra all exhibit a small desorption peak at ~475–490 °C as well an exponential increase in intensity starting at ~900 °C. Including m/e$^-$ 18, these are all the primary components of the QMS ionizer cracking pattern for CH_3OH.[135] The similarity in the spectra for these

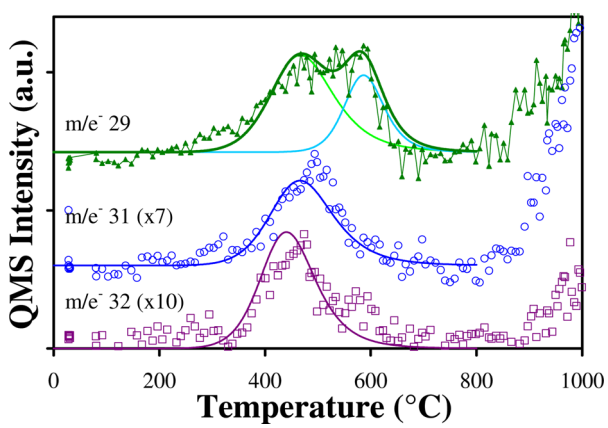

FIG. 8. (Color online) TPD spectrum from MeOH:BHF treated AlN surface for m/e$^-$ 29, 31, and 32. Symbols represent experimental data and lines fits to the experimental data derived using the described kinetic analysis.

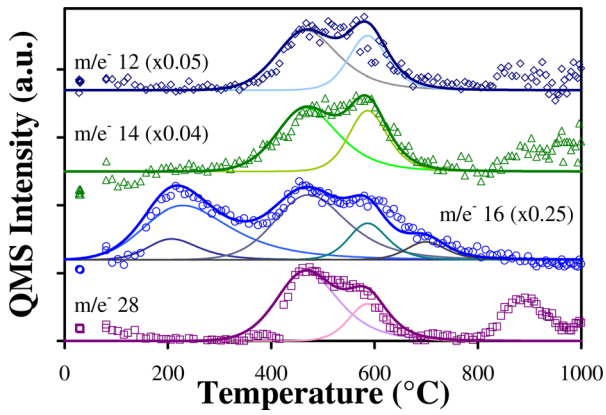

FIG. 9. (Color online) TPD spectrum from MeOH:BHF treated AlN surface for m/e$^-$ 12, 14, 16, and 28. Symbols represent experimental data and lines fits to the experimental data derived using the described kinetic analysis.

four m/e$^-$ ratios strongly supports their assignment to the desorption of CH_3OH as opposed to other possible species such as CO, CF, and O_2. It also suggests that at least part of the m/e$^-$ 18 signal may be due to H_2O^+ produced by ionizer fragmentation of desorbing CH_3OH as opposed to desorbing H_2O. As will discussed later, the higher temperature CH_3OH is more likely a result of recombinative desorption of surface CH_x and OH groups as opposed to CH_3OH adsorbed during the MeOH:BHF treatment. The observed desorption of CH_3OH at higher temperatures is also reasonably consistent with the post TPD XPS measurements where a decrease, but incomplete reduction in the C 1s intensity at 285.8 eV was observed [see Fig. 3(b)]. The surface carbon detected by XPS post TPD could be due to incomplete desorption of CH_3OH and other C species, or also due to re-absorption of CO, CO_2, and CH_3OH related species after completion of the TPD measurements and transfer to the XPS system.

Close inspection of the m/e$^-$ 29 spectra displayed in Fig. 8 also shows the possible presence of a second peak at ~590 °C that is not present for m/e$^-$ 18, 31, and 32. The close correspondence with the F_2 desorption peak at 585 °C suggests the origin of this peak is perhaps related to a F containing specie such as doubly ionized CF_3^{++} or $AlFC^{++}$. However, m/e$^-$ 29 also represents a small component of the ionizer fragmentation pattern for CO and N_2 in addition to CH_3OH. The observed m/e$^-$ 29/28 ratio (0.01) is close to that expected for both CO and N_2 and therefore the higher temperature peak for m/e$^-$ 29 could also be due to either CO or N_2 desorption.

Greater insight into the origin of the second m/e$^-$ 29 peak and the presence of other possible desorbing species can be gained by looking at m/e$^-$ 12 (C^+), 14 (N^+), 16 (O^+ or NH_2^+), and 28 (CO^+ and N_2^+). The TPD spectra for these four m/e$^-$ ratios are displayed in Fig. 9, and similar to m/e$^-$ 29, all four show a "square wave" like desorption feature starting at ~350 °C and finishing at 630 °C. The similar behavior for these m/e$^-$ ratios suggests that they are all possibly related to the same desorbing specie(s). Unfortunately, the observed ratios of m/e$^-$ 12 and 14 to 28 are both reasonably close to those expected for C^+/CO^+ and N^+/N_2^+ in the ionizer fragmentation patterns of CO and N_2, respectively. This again equally suggests both CO and N_2 desorption. The observed m/e$^-$ 16/28 ratio (0.25) is also slightly higher than that expected for O^+/CO^+ (0.1) from CO. Alternatively, some of the m/e$^-$ 16 signal could be due to ionizer fragmentation of desorbing NH_3, CO_2, or H_2O in the ionizer. The latter is a strong possibility as m/e$^-$ 16 clearly shows a similar desorption peak at 200 °C as for m/e$^-$ 18 in Fig. 6. However, the m/e$^-$ 16/18 ratio (0.5) is substantially larger than expected from H_2O. The m/e$^-$ 14/16 and 16/28 ratios are also substantially larger than those expected for the fragmentation patterns of NH_3 and CO_2, respectively. Greater clarity regarding NH_3 and CO_2 desorption could have been gained by monitoring the primary components for the ionizer fragmentation patterns of NH_3 (m/e$^-$ 17) and CO_2 (m/e$^-$ 44). Regrettably, these were not monitored due to data acquisition limitations.

Therefore, we cannot conclusively attribute the TPD spectra for m/e$^-$ 12, 14, 16, and 28 to desorption of purely NH_3, CO, N_2, or CO_2 based solely on the raw QMS data. Although we do note that desorption of all four and other related species is possible and perhaps likely. We also note that the observation of a signal for m/e$^-$ 12 does strongly suggest desorption of at least one C containing surface specie. Some intensity at m/e$^-$ 12 is certainly expected from 350 to 580 °C based on our previous assignment of CH_3OH desorption in this temperature range. It is also anticipated based on our prior combined thermal annealing and XPS measurements on BHF treated AlN surfaces where complete desorption of adventitious carbon species was clearly observed after annealing at 400–600 °C for 15 min.[73] This is in excellent agreement with our observation here that m/e$^-$ 12 returns to baseline levels by 630 °C. We also note that Pietsch *et al.*[77] and Kawase *et al.*[140] have observed desorption of C_xH_y and CF_x contaminants from HF and NH_4F treated Si (111) and (100) surfaces to occur in a similar temperature range of 400–600 °C. This is in agreement with the observation that m/e$^-$ 12, 14, 16, and 28 all show a TPD signal over a similar temperature range.

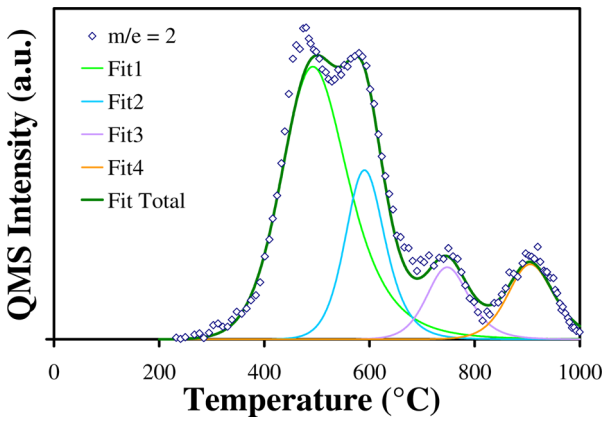

FIG. 10. (Color online) TPD spectrum from MeOH:BHF treated AlN surface for m/e$^-$ 2. Diamonds represent experimental data and lines fits to the experimental data derived using the described kinetic analysis.

Similarly, the observation of a signal for m/e$^-$ 14 strongly suggests desorption of a nitrogen containing specie. In this regard, we note that the MBMS study by Watanabe *et al.*[106,107] of XeF_2 thermal etching of AlN observed significant desorption of N_2 starting at temperatures of 500–600 °C, and the TPD study by Pietsch *et al.*[77] of NH_4F treated Si (111) surfaces observed desorption of N_xF_y species from 400 to 500 °C. The desorption of such species would be fully consistent with our observation of a TPD peak from 400 to 600 °C for m/e$^-$ 14 (N), 28 (N_2), and 38 (F_2). We also note that desorption of NH_3 from metal organic chemically vapor deposited (MOCVD) GaN has been reported by Shekhar and Jensen[141] and Ambacher *et al.*[142] to occur at 310 ± 20 °C and 500 ± 20 °C, respectively. The latter results from the Ambacher *et al.* study agree reasonably well with our TPD spectrum for m/e$^-$ 14 and 16.

Close inspection of the TPD spectrum for m/e$^-$ 28 in Fig. 9 also shows a desorption peak at ~900 °C that is not observed for any of the other monitored channels (except m/e$^-$ 2 as to be shown later). As previously discussed, it is difficult to assign m/e$^-$ 28 to a particular desorbing specie due to overlap with the fragmentation pattern of several different possible desorbing species (i.e., N_2 versus CO). However, based on the kinetic analysis of this peak that we will show later, we attribute this peak to desorption of N_2 directly liberated from the AlN film. The assignment of this high temperature desorption peak to N_2 is consistent with the slight increase in m/e$^-$ 14 from 800 to 1000 °C while m/e$^-$ 12 and 16 remain relatively flat over the same temperature range.

The TPD spectrum for m/e$^-$ 2 (H_2) is shown in Fig. 10 and exhibited multiple peaks at 480, 580, 760, and 910 °C that could be attributed to either direct recombinative H_2 desorption or H_2^+ ions produced by fragmentation of other desorbing species in the QMS ionizer. Based on similarities to the m/e$^-$ 18 TPD spectrum in Fig. 6, we attribute the m/e$^-$ 2 peak at 480 °C to H_2^+ produced by fragmentation of H_2O desorbing from AlOH surface groups. The m/e$^-$ 2 peak at 580 °C is attributed to NH_3 desorbing from N-H surfaces species as well as direct recombinative desorption of H_2 from surface N-H sites. This is based on prior TPD investigations of GaN (0001) surfaces where D_2 was observed to desorb from surface N-D species at 400–500 °C,[141,143] and NH_3 at 350–780 °C.[142] For the H_2 desorption peaks at 760 and 910 °C, we attribute these to H_2^+ produced by fragmentation of H_2O and/or recombinative desorption of H_2 from isolated OH surface or subsurface groups. These assignments are based primarily on the exponential increase in H_2O desorption observed starting at these temperatures, and the TPD study by Shirai that showed H_2O desorption from isolated AlOH surface groups on Al_2O_3 powders at similar temperatures.[136] We do note here that the highest temperature desorption peak may also be attributed to outgassing of H_2 dissolved in the AlN film and/or due to H_2 liberated in sublimation of the AlN film. Additional support for all of these assignments will be provided in Sec. III B based on a more detailed kinetic analysis of the TPD spectra for m/e$^-$ 2, 16, and 18.

Referencing the intensity of the detected desorbing species to the previously measured integrated intensity of hydrogen desorption from a fully hydrogenated Si (111) surface[121] indicated desorption of approximately 9, 2.7, and 1.5 × 10^{15} H_2, H_2O, and HF molecules/cm^2. The observed intensity for m/e$^-$ 28 was ~7 × 10^{15} molecules/cm^2. The integrated intensity for the other observed species desorbing was <0.5 × 10^{15} molecules/cm^2. For comparison, Tompkins has observed desorption of ~10–100 × 10^{15}/cm^2 H_2O molecules from spin-coated and plasma deposited SiO_2 films.[78–80]

B. TPD kinetic analysis

More detailed analysis of the TPD spectra for m/e$^-$ 2, 18, 19, 20, 31, and 38, and portions of m/e$^-$ 16 and 28 were performed in order to determine the activation energy and preexponential for desorption of H_2, H_2O, F, HF, MeOH, F_2, NH_3, and N_2, respectively, from AlN surfaces. The results of this analysis are summarized in Table II. A detailed kinetic analysis was not attempted for the m/e$^-$ 12, 14, 16, 28, and 29 TPD spectra from 350 to 630 °C due to the square wave nature of the features in this region, and an inability to conclusively assign their origin. However, as we will show later,

TABLE II. Summary of kinetic parameters for desorption of various species from AlN surfaces determined in this study.

m/e$^-$	Desorbing specie	T_{max} (°C)	E_d (kJ/mol)	ν_d (cm^2/s)
2	H_2, H_2O, CH_3OH	480	106 ± 5	1.5 ± 5 × 10^{-10}
	H_2, NH_3	580	230 ± 20	1.0 × $10^{-3\pm1}$
	H_2O	760	305 ± 30	5 × $10^{-2\pm1}$
	H_2	910	370 ± 20	0.4 ± 0.2
16	NH_x	205	30 ± 5	$10^{-15\pm1}$
18	H_2O	195	51 ± 3	4 ± 4 × 10^{-12}
	H_2O	460	87 ± 5	8.0 ± 5 × 10^{-12}
19	F, AlF_x, N_xF_y	530	62 ± 5	5 ± 5 × 10^{-14}
20	HF, AlF_x, N_xF_y	475	110 ± 5	4 ± 4 × 10^{-10}
28	N_2	880	535 ± 30	2 ± 1 × 10^7
31	CH_3OH, CF	490	102 ± 5	2 ± 5 × 10^{-10}
32	CH_3OH, O_2	480	110 ± 5	2 ± 5 × 10^{-10}
38	F_2, AlF_x, N_xF_y	485	62 ± 3	4 ± 5 × 10^{-10}
		585	270 ± 10	1 ± 0.5

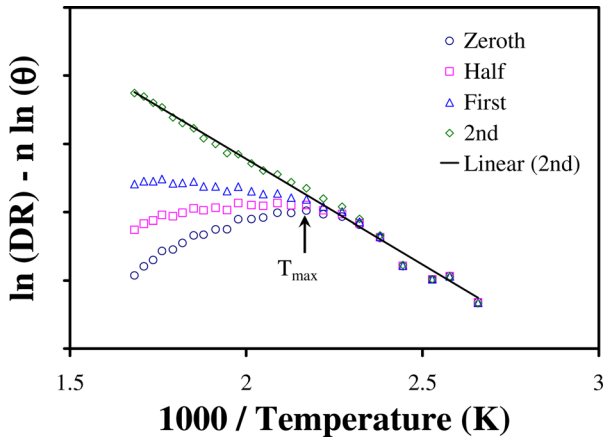

FIG. 11. (Color online) Kinetic analysis described in text for m/e$^-$ 18 peak at 190 °C for zeroth, half, first, and second order desorption kinetics.

these portions of the spectra were well fitted using the kinetic parameters derived for m/e$^-$ 2 and 20 in this temperature range.

Figure 11 shows a plot of ln (DR) versus 1/T for m/e$^-$ 18 covering the low temperature desorption peak observed at 195 °C. As can be seen, second order kinetics yields a straight line with an R^2 of 0.99. The activation energy and pre-exponential for desorption extracted from the slope and y-intercept of Fig. 11 were $E_d = 51 \pm 3$ kJ/mol and $\nu_d = 4 \pm 4 \times 10^{-12}$ cm^2/s, respectively. These values are in reasonable agreement with the values of $E_d = 62$ kJ/mol and $\nu_d = 7.3 \times 10^{-10}$ cm^2/s obtained by Schildbach using a similar analysis for second order H_2O desorption kinetics from nonpolar Al_2O_3 (11$\bar{2}$0) surfaces.[116] The activation energy for desorption determined here is also in excellent agreement with the value of $E_d = 55 \pm 17$ kJ/mol determined by Proost *et al.* for desorption of tightly hydrogen bonded water from a spin-on SiO_2 film, and the reported hydroxyl–water binding energy of 60 kJ/mol.[84] A similar kinetic analysis was also performed for the higher temperature H_2O desorption peak observed at 460 °C. That analysis (not shown) also indicated second order desorption kinetics with $E_d = 87 \pm 5$ kJ/mol and $\nu_d = 8 \pm 5 \times 10^{-12}$ cm^2/s, respectively. The value of E_d determined for this higher temperature H_2O desorption peak is consistent

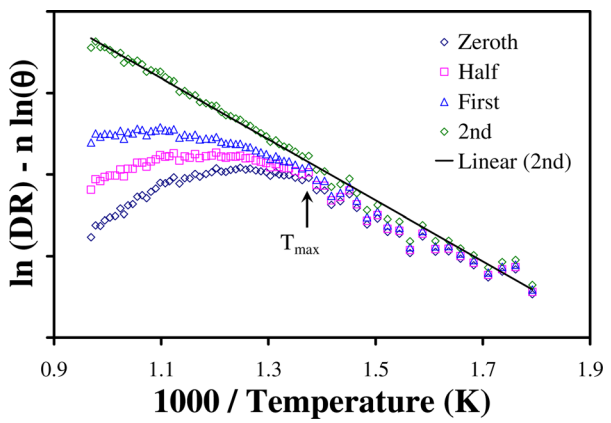

FIG. 12. (Color online) Kinetic analysis described in text for m/e$^-$ 19 for zeroth, half, first, and second order desorption kinetics.

with the lower range of 96–170 kJ/mol determined by Nelson *et al.* for first order desorption of H_2O from OH groups on Al_2O_3 (0001) surfaces.[117,118] It is also in excellent agreement with the values of 80 and 89 ± 1 kJ/mol determined by Tompkins and Deal[82] and Proost *et al.*,[84] respectively, for H_2O desorption from hydrogen bonded silanol groups in spin-on deposited SiO_2 films.[84]

These similarities reasonably confirm our assignment of the two H_2O desorption peaks at 195 and 460 °C to desorption of physisorbed/hydrogen bonded water and H_2O desorption from surface AlOOH and AlOH species, respectively. Figure 6 shows the measured m/e$^-$ 18 TPD spectrum with the predicted desorption spectra based on the above kinetic analysis. As can be seen, the kinetic modeling well describes/fits the observed desorption spectrum.

Figure 12 shows a plot of ln (DR) versus 1/T for m/e$^-$ 19 (F). As can be seen, second order kinetics yields a straight line with an R^2 of 0.98. The activation energy and pre-exponential for desorption extracted from the slope and y-intercept of Fig. 12 were $E_d = 62 \pm 5$ kJ/mol and $\nu_d = 5 \pm 5 \times 10^{-14}$ cm^2/s, respectively. A similar plot for m/e$^-$ 20 also indicated second order kinetics but with a substantially higher E_d of 110 ± 5 kJ/mol and $\nu_d = 4 \pm 5 \times 10^{-10}$ cm^2/s. The value of 110 kJ/mol for m/e$^-$ 20 desorption is in excellent agreement with the value of 105.9 ± 3 kJ/mol previously determined by Watanabe *et al.* for AlF_x formation and desorption from AlN surfaces thermally etched by XeF_2.[106,108] This suggests the possibility that in addition to HF, the m/e$^-$ 20 signal may also represent a component of the ionizer fragmentation for desorbing AlF_x species.

As shown in Fig. 7, the TPD spectrum for m/e$^-$ 38 exhibited two different desorption peaks at 485 and 585 °C. A plot of ln (DR) versus 1/T for the higher temperature desorption peak at 585 °C indicated second order desorption with $E_d = 270 \pm 10$ kJ/mol and $\nu_d = 1 \pm 0.5$ cm^2/s. This E_d value is again in excellent agreement with the value of 272 ± 4 kJ/mol previously determined by Watanabe *et al.* for desorption of AlF_2 from an AlF_3 film formed on Al_2O_3.[108] As shown in Fig. 7, the lower temperature peak for m/e$^-$ 38 was well described using the kinetic parameters previously determined for m/e$^-$ 19. This indicates that m/e$^-$ 19 and the lower temperature m/e$^-$ 38 peak are likely related to the same desorbing specie, which is most probably AlF_x based on the prior study by Watanabe *et al.*[106,108]

Kinetic analysis for the m/e$^-$ 31 and 32 TPD spectra both indicated second order desorption kinetics and yielded virtually identical results of $E_d = 105 \pm 5$ kJ/mol and $\nu_d = 2 \pm 5 \times 10^{-10}$ cm^2/s. These results are extremely similar to those determined for m/e$^-$ 20 and suggest similar origins. In this regard, we do note that m/e$^-$ 31 and 32 could alternatively represent CF^+ and CFH^+ species. For carbon contaminated HF processed Si (111) wafers, Pietsch *et al.* has previously reported desorption of both C_xH_y (m/e$^-$ 12–16, 24–30, 36–46) and CF_x [m/e$^-$ 31 (CF^+) and m/e$^-$ 50 (CF_2^+)] species at temperatures of 400–600 °C.[77] The CF_x species were postulated to have originated from the reaction of HF with surface carbon. However, the presence of such CF_x surface species were not noticed in the pre-TPD XPS C 1s

measurements, and Ambacher *et al*. has previously determined an E_d of 182 kJ/mol for desorption of C_xH_y species at ~375 °C from ambient exposed MOCVD AlN films.[142]

For m/e$^-$ 2 (H_2), the overlap of multiple peaks allowed a detailed kinetic analysis to be performed for only the lowest and highest temperature peaks observed. For the lowest temperature peak at 480 °C, second order desorption kinetics were determined with $E_d = 106 \pm 5$ kJ/mol and $\nu_d = 1.4 \times 10^{-10}$ cm^2/s. This is again very similar to the E_d determined for m/e$^-$ 20, 31, and 32 and suggests that this is possibly due to H_2^+ produced by ionizer fragmentation of HF and CH_3OH. As H_2O desorption was also observed to peak at 460 °C with fairly similar kinetic parameters, a portion of the H_2 desorption peak at 480 °C is also likely due to H_2O desorption.

For the second and third m/e$^-$ 2 peaks in Fig. 10 at 580 and 760 °C, respectively, a detailed kinetic analysis was not possible due to significant peak overlap. However, we empirically found that $E_d = 230 \pm 20$ kJ/mol ($\nu_d = 1 \times 10^{-3 \pm 1}$cm^2/s) and 305 ± 30 kJ/mol ($\nu_d = 0.05 \pm 0.05$ cm^2/s) adequately fitted the peaks at 580 and 760 °C, respectively (see Fig. 10). The former is in reasonable agreement with the upper range value of 171 kJ/mol determined by Nelson *et al*.[117] for H_2O desorption from Al_2O_3 (0001), and the value of 202 ± 18 kJ/mol determined by Proost *et al*. for H_2O desorption from isolated silanol sites.[77] However, there is no clear m/e$^-$ 18/H_2O desorption peak at 580 °C. Alternatively, the 580 °C peak could be due to direct recombinative desorption of H_2 from N-H surface species, or H_2^+ produced in the QMS ionizer by desorbing NH_3. For the former, the above value is in excellent agreement with the E_d of 230 kJ/mol that we previously estimated for H_2 desorption from N-H surface species on AlN and GaN surfaces based on the similarities in Si-H and N-H bond energies and the activation energy for H_2 desorption from Si surfaces.[124] For the latter, the E_d of 230 kJ/mol is bracketed by the experimental E_d of 220–260 kJ/mol reported by Ambacher *et al*. for NH_3 desorption from GaN,[142] and the theoretical value of 240 kJ/mol calculated by Panyukova for NH_3 desorption from the nitrogen face of AlN (0001).[144] Attribution of the 580 °C m/e$^-$ 2 peak to NH_3 desorption is also consistent with a minor peak at 580–590 °C for the m/e$^-$ 14 (N^+) and 16 (NH_2^+) TPD spectra that, as shown in Fig. 9, are well fitted using the same kinetic parameters. Therefore, we tentatively attribute the m/e$^-$ 2 peak at 580 °C to H_2 desorption from either N-H surface species and/or H_2^+ created by ionizer fragmentation of desorbing NH_3.

For the m/e$^-$ 2 desorption peak at 760 °C, we note that the estimated E_d of 305 ± 30 kJ/mol is intermediate between the value of 202 ± 18 determined by Proost *et al*. for H_2O desorption from isolated silanols at 631 °C,[77] and the value 370 kJ/mol determined by Ambacher *et al*. for O_2 desorption from AlN at 1017 °C.[142] As the exponential increase in m/e$^-$ 18/H_2O desorption intensity starts at ~740 °C, we tentatively attribute this third peak to H_2O desorption from isolated OH groups on the AlN surface. Attribution of this peak to H_2O desorption is also consistent with a small peak observed at a similar temperature for m/e$^-$ 16 (i.e., O^+). As shown in Fig. 9, this peak was well fitted using similar kinetic parameters as for the 760 °C H_2 peak.

For the highest temperature m/e$^-$ 2 peak observed at 910 °C, a more rigorous kinetic analysis was possible and indicated second order kinetics with $E_d = 370 \pm 20$ kJ/mol and $\nu_d = 0.4 \pm 0.2$ cm^2/s. The E_d for the highest temperature m/e$^-$ 2 TPD peak aligns well with the previously mentioned value of 370 kJ/mol for O_2 desorption from AlN,[142] and the value of 399 kJ/mol determined by Kumagi for the decomposition of MOCVD AlN (0001) films in flowing H_2.[145] The close correspondence with the E_d for O_2 desorption from AlN determined by Ambacher *et al*. suggests that the m/e$^-$ 2 peak at 910 °C is related to some H_2 liberated during the desorption of O_2 from the AlN surface. This is consistent with the observed exponential increase in intensity for m/e$^-$ 32 (i.e., possibly O_2^+) starting at 890–900 °C, and suggests that dehydration of isolated surface OH may also occur via O_2 and H_2 desorption at higher temperatures.

The similarity of the E_d values for H_2 and O_2 desorption from AlN to the activation energy for AlN sublimation determined by Kumagi also suggests that some sublimation or decomposition of AlN may be accompanied with H_2 and O_2 desorption. AlN sublimation is generally believed to occur via the following reaction:

$$\mathrm{AlN(s)} = \mathrm{Al(g)} + 1/2\mathrm{N_2(g)}, \tag{3}$$

where (s) and (g) refer to solid and gas phases.[145] Thus, sublimation of AlN should be accompanied by the release of some detectable N_2 at m/e$^-$ 28. In this regard, we do note that a high temperature peak was observed for m/e$^-$ 28 at ~900 °C. Kinetic analysis of this peak, however, indicated a much higher E_d of 535 ± 30 kJ/mol ($v_d = 2 \pm 1 \times 10^7$ cm^2/s). Though substantially different from that determined for the m/e$^-$ 2 peak at 910 °C, this value is in excellent agreement with the value of 520 ± 30 kJ/mol determined by Fan for the sublimation of AlN (0001) films grown on 6 H-SiC (0001) substrates via reactive molecular beam epitaxy.[146]

The discrepancies in reported E_d for AlN sublimation can be understood by considering a few key differences between the different experiments. First, Kumagi investigated the sublimation of air exposed AlN thin films under flowing H_2 at atmospheric pressure. In contrast, Fan investigated the sublimation of freshly grown AlN films under UHV conditions. For the former, Kumagi postulated that sublimation occurs via the reaction: $\mathrm{AlN(s)} + \mathrm{H_2(g)} \rightarrow \mathrm{AlH_x(g)} + \mathrm{NH_3(g)}$. For the UHV conditions utilized in the Fan study though, it is more reasonable to expect AlN sublimation to occur via Eq. (3) above. In our case, we postulate that some decomposition of the native oxide on the surface of the AlN film occurred via: $\mathrm{AlOH} \rightarrow \mathrm{Al(g)} + \mathrm{H_2(g)} + \mathrm{O_2(g)}$. Thus, the m/e$^-$ 2/H_2 peak observed at 910 °C could be due to H_2 assisted decomposition of AlN or surface AlO_x species, where as the m/e$^-$ 28 peak at ~900 °C could represent direct AlN sublimation. However, we should note that both peaks are substantially below the temperatures of 1100–1400 °C utilized by Kumagi and Fan to study AlN sublimation. In this regard, we do note that Fan observed enhanced evaporation at dislocation sites at lower temperatures. Therefore, it is possible that the

desorption observed here is due to sublimation from line defects or grain boundaries in the AlN film.

As mentioned previously, a detailed kinetic analysis was not attempted for the square wave feature exhibited by m/e^- 12, 14, 16, 28, and 29 at 350–630 °C. However, as we show in Figs. 8 and 9, these features were all reasonably well fitted using the E_d and ν_d previously determined for HF and H_2 desorption. Although we note that m/e^- 12 suggests the desorption of some CH_xF_y, and C_xH_y species, we primarily attribute these features to the collective desorption of N_2, NH_3, and NH_xF_y species. The assignment of N_2 desorption is clearly supported by the prior MBMS study of Watanabe *et al*. that showed N_2 and AlF_3 to be the primary desorbing etch products in the thermal reaction of XeF_2 with AlN in the temperature range of 500–600 °C.[106,108] Our observations of the presence of AlF_x in XPS pre-TPD and of desorbing F_2 exhibiting a similar E_d to that measured by Watanabe *et al*. for AlF_3, therefore, implies N_2 desorption and is further supported by the observed signals at m/e^- 14 (N^+) and 28 (N_2^+). Although NH_3 was not observed to be a major desorbing product in the Watanabe *et al*. study, desorption of NH_3 is clearly supported in this study by the observed signals at m/e^- 14 and 16 (NH_2^+) and the comparable values of E_d for NH_3 desorption reported by Ambacher *et al*. and that determined here for H_2 desorption at 585 °C.[142] We also note that the formation of NH_3 desorption products is more likely in our study due to the higher concentration of surface hydroxides relative to the Watanabe *et al*. study where the hydroxides could contribute hydrogen to dangling N bonds, i.e., $AlOH + \bullet N \rightarrow AlO + NH$. Similarly, the desorption of NH_xF_y species is supported by the pre- and post-XPS measurements and the ability of surface hydroxides to contribute hydrogen to surface NF_x species.

Further support for desorption of NH_x related species from the AlN surfaces is provided by a kinetic analysis of the low temperature peak observed at 205 °C for m/e^- 16. Although m/e^- 18 exhibits a similar peak at 195 °C and ionizer fragmentation of desorbing H_2O should produce a signal at m/e^- 16, the kinetic analysis indicates significantly different values of $E_d = 30 \pm 5$ kJ/mol and $\nu_d = 10^{-15\pm1}$ cm^2/s, suggesting that the m/e^- 16 feature at 205 °C is not completely related to that for m/e^- 18. In this regard, we note that Pietsch *et al*. has reported the desorption of NH_4 at 100–200 °C from NH_4F processed Si (111) surfaces.[77] Therefore, the derived kinetic parameters are likely more related to desorption of physisorbed NH_4. However, as shown in Fig. 9, the derived kinetic parameter for this m/e^- 16 peak do not adequately reproduce the experimental data. To obtain a more satisfying fit, we found it necessary to include an additional peak utilizing the kinetic parameters determined for the m/e^- 18 peak at 195 °C. Therefore, the m/e^- 16 TPD spectrum likely represents a combination of both H_2O and NH_x desorption.

Lastly, some comment is merited regarding the observation of second-order desorption kinetics for all the species monitored in this investigation relative to the numerous reports of first order desorption kinetics shown in Table I. Both first and second order kinetics are dependent on the instantaneous surface coverage of species. However, the θ^2 dependence for second order desorption implies desorption occurs via a recombinatory mechanism between neighboring surface species and more specifically indicates that desorption is limited by the availability of a neighboring surface specie for recombinantory desorption. The latter is an important consideration for covalent material surfaces where the mobility of surface species is greatly reduced and (barring a few notable exceptions[147]) consistent with the predominant observation of second order desorption kinetics on other covalent materials surfaces such as diamond, silicon, and silicon carbide.[127] In this regard, assumptions of first order kinetics for desorption from covalent surfaces are somewhat speculative and dubious. For the few cases in Table I where the desorption kinetics were not assumed to be first order, second order kinetics were determined as in this study.

IV. SUMMARY AND CONCLUSIONS

In summary, XPS and TPD were utilized to investigate desorption of various species from AlN surfaces fluorinated in a 1:1 MeOH:BHF solution. The primary species observed desorbing were H_2O, HF, F_2, CH_3OH, N_2, and NH_3. A detailed kinetic analysis of the TPD spectra indicated second order desorption kinetics in all cases, and the determined activation energies for desorption were found to be in agreement with studies of similar species desorbing from related surfaces (see Tables I and II). While some low temperature desorption of physisorbed H_2O and NH_4 was observed to occur from 100 to 300 °C, the majority of the desorbing species was observed to occur in the temperature range of 350–630 °C with nearly identical E_d of 110 ± 5 and 230 ± 20 kJ/mol. Some desorption of H_2 and N_2 at 800–970 °C was also observed with E_d of 370 ± 20 and 535 ± 30 kJ/mol. The latter are consistent with H_2 assisted and direct sublimation of AlN, respectively.

ACKNOWLEDGMENTS

The authors would like to thank Z. Redzimski for supplying the AlN film utilized in this study. This work was supported by the ONR under Contract Nos. N00014-91-J-1410 and N00014-92-J1477, and by the Department of Education through an Electronic Materials Fellowship.

[1]R. Waits, J. Vac. Sci. Technol., A **18**, 1736 (2000).
[2]S. King, H. Simka, D. Herr, H. Akinaga, and M. Garner, APL Mater. **1**, 040701 (2013).
[3]G. Pietsch, Appl. Phys. A **60**, 347 (1995).
[4]W. Kern, RCA Rev. **39**, 278 (1978).
[5]*Handbook of Si Wafer Cleaning Technology*, 2nd ed., edited by K. Reinhardt and W. Kern (William Andrew Inc., Norwich, NY, 2008).
[6]M. Sekine, Appl. Surf. Sci. **192**, 270 (2002).
[7]C. Cardinaud, M. Peignon, and P. Tessier, Appl. Surf. Sci. **164**, 72 (2000).
[8]H. Abe, M. Yoneda, and N. Fujiwara, Jpn. J. Appl. Phys., Part 1 **47**, 1435 (2008).
[9]W. Kern, J. Electrochem. Soc. **137**, 1887 (1990).
[10]D. Flamm and V. Donnelly, Plasma Chem. Plasma Process. **1**, 317 (1981).
[11]D. Flamm, V. Donnelly, and D. Ibbotson, J. Vac. Sci. Technol., B **1**, 23 (1983).
[12]Y. Chabal, G. Higashi, K. Raghavachari, and V. Burrows, J. Vac. Sci. Technol., A **7**, 2104 (1989).

[13]T. Ohmi, J. Electrochem. Soc. **143**, 2957 (1996).
[14]H. Okorn-Schmidt, IBM J. Res. Dev. **43**, 351 (1999).
[15]F. Pease, J. Vac. Sci. Technol., B **28**, C6A1 (2010).
[16]J. Coburn and H. Winters, J. Vac. Sci. Technol. **16**, 391 (1979).
[17]G. Oehrlein, M. Doemling, B. Kastenmeier, P. Matsuo, N. Rueger, M. Schaepkens, and T. Standaert, IBM J. Res. Dev. **43**, 181 (1999).
[18]M. Hori and T. Goto, Appl. Surf. Sci. **192**, 135 (2002).
[19]J. Coburn and H. Winters, J. Appl. Phys. **50**, 3189 (1979).
[20]E. Fisher, Plasma Sources Sci. Technol. **11**, A105 (2002).
[21]Y. Osano and K. Ono, Jpn. J. Appl. Phys., Part 1 **44**, 8650 (2005).
[22]V. Donnelly, J. Guha, and L. Stafford, J. Vac. Sci. Technol., A **29**, 010801 (2011).
[23]M. Houston and R. Maboudian, J. Appl. Phys. **78**, 3801 (1995).
[24]Y. Kawabata and S. Adachi, Appl. Surf. Sci., **152**, 177 (1999).
[25]Z. Lu, C. Lagarde, E. Sacher, J. Currie, and A. Yelon, J. Vac. Sci. Technol., A **7**, 646 (1989).
[26]T. Smith, Surf. Sci. **32**, 527 (1972).
[27]D. Hess, Plasma Chem. Plasma Process. **2**, 141 (1982).
[28]D. Smith and R. Bruce, J. Electrochem. Soc. **129**, 2045 (1982).
[29]D. Smith and P. Saviano, J. Vac. Sci. Technol. **21**, 768 (1982).
[30]R. Janssen, A. Kolfschoten, and G. van Veen, Appl. Phys. Lett. **52**, 98 (1988).
[31]V. Bermudez and A. Glass, J. Vac. Sci. Technol., A **7**, 1961 (1989).
[32]P. Gupta, P. Coon, B. Koehler, and S. George, J. Chem. Phys. **93**, 2827 (1990).
[33]R. Carlile, V. Liang, O. Palusinski, and M. Smadi, J. Electrochem. Soc. **135**, 2058 (1988).
[34]P. Gadgil, D. Dane, and T. Maneti, J. Vac. Sci. Technol., A **10**, 1303 (1992).
[35]L. DeLouise, J. Appl. Phys. **70**, 1718 (1991).
[36]H. Flaum, D. Sullivan, and A. Kummel, J. Chem. Phys. **100**, 1634 (1994).
[37]J. Engstrom, M. Nelson, and T. Engel, Phys. Rev. B **37**, 6563 (1988).
[38]S. Vanhaelemeersch, J. Van Hoeymissen, D. Vermeylen, and J. Peeters, J. Appl. Phys. **70**, 3892 (1991).
[39]D. Gray, I. Tepermeister, and H. Sawin, J. Vac. Sci. Technol., B **11**, 1243 (1993).
[40]G. Oehrlein and H. Williams, J. Appl. Phys. **62**, 662 (1987).
[41]O. Kwon and H. Sawin, J. Vac. Sci. Technol., A **24**, 1906 (2006).
[42]J. Butterbaugh, D. Gray, and H. Sawin, J. Vac. Sci. Technol., B **9**, 1461 (1991).
[43]N. Ikegami, Y. Miyakawa, J. Hashimoto, N. Ozawa, and J. Kanamori, Jpn. J. Appl. Phys., Part 1 **32**, 6088 (1993).
[44]Z. He and K. Leung, Appl. Surf. Sci. **174**, 225 (2001).
[45]Y. Kuo, J. Vac. Sci. Technol., A **8**, 1702 (1990).
[46]J. Lee, G. Lee, J. Min, and S. Moon, J. Vac. Sci. Technol., A **25**, 1395 (2007).
[47]M. Schaepkens, T. Standaert, N. Rueger, P. Sebel, and G. Oehrlein, J. Vac. Sci. Technol., A **17**, 26 (1999).
[48]F. Weilnboeck, E. Bartis, S. Shachar, G. Oehrlein, D. Farber, T. Lii, and C. Lenox, J. Vac. Sci. Technol., B **30**, 41811 (2012).
[49]M. Fukasawa, T. Tatsumi, K. Oshima, K. Nagahata, S. Uchida, S. Takashima, M. Hori, and Y. Kamide, J. Vac. Sci. Technol., A **26**, 870 (2008).
[50]G. Oehrlein, J. Rembetski, and E. Payne, J. Vac. Sci. Technol., B **8**, 1199 (1990).
[51]H. Haverlag, G. Oehrlein, and D. Vender, J. Vac. Sci. Technol., B **12**, 96 (1994).
[52]T. Standaert, M. Schaepkens, N. Rueger, P. Sebel, G. Oehrlein, and J. Cook, J. Vac. Sci. Technol., A **16**, 239 (1998).
[53]T. Standaert, C. Hedlund, E. Joseph, G. Oehrlein, and T. Dalton, J. Vac. Sci. Technol., A **22**, 53 (2004).
[54]V. Raballand, G. Cartry, and C. Cardinaud, J. Appl. Phys. **102**, 063306 (2007).
[55]R. Khare, A. Srivastava, and V. Donnelly, J. Vac. Sci. Technol., A **30**, 051307 (2012).
[56]R. Khare, A. Srivastava, and V. Donnelly, J. Vac. Sci. Technol., A **30**, 051306 (2012).
[57]X. Li, H. Ling, G. Oehrlein, E. Karwacki, and B. Ji, J. Vac. Sci. Technol., A **22**, 158 (2004).
[58]S. Ullal, H. Singh, J. Daugherty, V. Vahedi, and E. Aydil, J. Vac. Sci. Technol., A **20**, 1195 (2002).
[59]A. Zhao, J. Bulger, L. Green, W. Harris, T. Hunt, W. Marchesseault, M. French, and H. Lisy, "Improvement of film uniformity stability of pecvd silicon nitride deposition process by addition of fluorine to the plasma clean sequence," *Advance Semiconductor Manufacturing Conference*, Munich, Germany, 11–12 April (2005), pp. 143–148.
[60]C. Whelan, J. Bulger, A. Dumont, J. Clark, and M. Kuhn, J. Vac. Sci. Technol., B **17**, 194 (1999).
[61]B. Smith and A. Young, J. Electrochem. Soc. **148**, C721 (2001).
[62]N. Ito, T. Moriya, F. Uesugi, M. Matsumoto, S. Liu, and Y. Kitayama, Jpn. J. Appl. Phys., Part 1 **47**, 3630 (2008).
[63]M. Blain, G. Tipton, W. Holber, G. Selwyn, P. Westerfield, and K. Maxwell, Plasma Sources Sci. Technol. **3**, 325 (1994).
[64]J. Logan and J. McGill, J. Vac. Sci. Technol., A **10**, 1875 (1992).
[65]G. Selwyn, J. Vac. Sci. Technol., B **9**, 3487 (1991).
[66]J. O'Hanlon and H. Parks, J. Vac. Sci. Technol., A **10**, 1863 (1992).
[67]N. Miki, M. Maeno, K. Maruhashi, Y. Nakagawa, and T. Ohmi, IEEE Trans. Semicond. Manuf. **3**, 1 (1990).
[68]M. Maeno, Y. Nakagawa, N. Miki, and T. Ohmi, IEEE Trans. Semicond. Manuf. **5**, 107 (1992).
[69]P. Thiel, Surf. Sci. Rep. **7**, 211 (1987).
[70]M. Henderson, Surf. Sci. Rep. **46**, 1 (2002).
[71]R. Dalmau, R. Collazo, S. Mita, and Z. Sitar, J. Electron. Mater. **36**, 414 (2007).
[72]I. Bryan, C. Akouala, J. Tweedie, Z. Bryan, A. Rice, R. Kriste, R. Collazo, and Z. Sitar, Phys. Status Solidi C **11**, 454 (2014).
[73]S. King, J. Barnak, M. Bremser, K. Tracy, C. Ronning, R. Davis, and R. Nemanich, J. Appl. Phys. **84**, 5248 (1998).
[74]S. King, M. Benjamin, R. Nemanich, R. Davis, and W. Lambrecht, MRS Proc. **395**, 739 (1996).
[75]L. Svedberg, K. Arndt, and M. Cima, J. Am. Ceram. Soc. **83**, 41 (2000).
[76]A. Rice, R. Collazo, J. Tweedie, R. Dalmau, S. Mita, J. Xie, and Z. Sitar, J. Appl. Phys. **108**, 043510 (2010).
[77]G. Pietsch, U. Kohler, and M. Henzler, J. Vac. Sci. Technol., B **12**, 78 (1994).
[78]H. Tompkins and C. Tracy, J. Electrochem. Soc. **136**, 2331 (1989).
[79]H. Tompkins and C. Tracy, J. Vac. Sci. Technol., B **8**, 558 (1990).
[80]H. Tompkins, G. Grivna, W. Cowden, and C. Leathersich, J. Vac. Sci. Technol., B **9**, 2738 (1991).
[81]R. Sokoll, H. Tiller, and T. Hoyer, J. Electrochem. Soc. **138**, 2150 (1991).
[82]H. Tompkins and P. Deal, J. Vac. Sci. Technol., B **11**, 727 (1993).
[83]N. Hirashita, S. Tokitoh, and H. Uchida, Jpn. J. Appl. Phys., Part 1 **32**, 1787 (1993).
[84]J. Proost, E. Kondoh, G. Vereecke, M. Heyns, and K. Maex, J. Vac. Sci. Technol., B **16**, 2091 (1998).
[85]D. Cheng, K. Tsukamoto, H. Komiyama, Y. Nishimoto, N. Tokumasu, and K. Maeda, J. Appl. Phys. **85**, 7140 (1999).
[86]J. Proost, M. Baklanov, K. Maex, and L. Delaey, J. Vac. Sci. Technol., B **18**, 303 (2000).
[87]T. Chang*et al.*, Electrochem. Solid-State Lett. **6**, F13 (2003).
[88]N. Biswas, J. Lubguban, and S. Gangopadhyay, Appl. Phys. Lett. **84**, 4254 (2004).
[89]A. Singh, P. Victor, P. Ganesan, O. Nalamasu, and G. Ramanath, Appl. Phys. Lett. **87**, 253506 (2005).
[90]Y. Li, I. Ciofi, L. Carbonell, N. Heylen, J. Van Aelst, M. Baklanov, G. Groeseneken, K. Maex, and Z. Tokei, J. Appl. Phys. **104**, 034113 (2008).
[91]C. Kubasch, C. Klaus, H. Ruelke, U. Mayer, and J. Bartha, IEEE Trans. Electron Devices **57**, 1865 (2010).
[92]E. Liniger, T. Shaw, S. Cohen, P. Leung, S. Gates, G. Bonilla, D. Canaperi, and S. Rao, Microelectron. Eng. **92**, 130 (2012).
[93]X. Guo, J. Jakes, S. Banna, Y. Nishi, and J. Shohet, J. Vac. Sci. Technol., A **32**, 031512 (2014).
[94]Y. Cheng, K. Leon, J. Huang, W. Chang, Y. Chang, and J. Leu, Microelectron. Eng. **114**, 12 (2014).
[95]S. Pearton, C. Abernathy, and F. Ren, Appl. Phys. Lett. **64**, 3643 (1994).
[96]K. Kolari, Microelectron. Eng. **85**, 985 (2008).
[97]S. Smith, C. Wolden, M. Bremser, A. Hanser, R. Davis, and W. Lampert, Appl. Phys. Lett. **71**, 3631 (1997).
[98]F. Khan, L. Zhou, V. Kumar, I. Adesida, and R. Okojie, Mater. Sci. Eng., B **95**, 51 (2002).
[99]G. Cunge, B. Pelissier, O. Joubert, R. Ramos, and C. Maurice, Plasma Sources Sci. Technol. **14**, 599 (2005).
[100]R. Ramos, G. Cunge, B. Pelissier, and O. Joubert, Plasma Sources Sci. Technol. **16**, 711 (2007).
[101]R. Ramos, G. Cunge, O. Joubert, N. Sadeghi, M. Mori, and L. Vallier, Thin Solid Films **515**, 4846 (2007).

[102]S. Raoux *et al.*, J. Vac. Sci. Technol., B **17**, 477 (1999).
[103]H. Aoki, Y. Teraoka, E. Ikawa, T. Kikkawa, and I. Nishiyama, J. Vac. Sci. Technol., A **13**, 42 (1995).
[104]M. Yu, K. Ahn, and R. Joshi, J. Appl. Phys. **67**, 1055 (1990).
[105]L. Vergara, R. Vidal, J. Ferron, E. Sanchez, and O. Grizzi, Surf. Sci. **482–485**, 854 (2001).
[106]M. Watanabe, T. Iida, K. Akiyama, S. Narita, T. Ishikawa, H. Sakai, K. Sawabe, and K. Shobatake, Jpn. J. Appl. Phys., Part 2 **42**, L356 (2003).
[107]M. Watanabe, Y. Mori, T. Ishikawa, H. Sakai, T. Iida, K. Akiyama, S. Narita, K. Sawabe, and K. Shobatake, J. Vac. Sci. Technol., A **23**, 1647 (2005).
[108]M. Watanabe, T. Iida, K. Akiyama, T. Ishikawa, H. Sakai, K. Sawabe, and K. Shobatake, Jpn. J. Appl. Phys., Part 2 **42**, L680 (2003).
[109]S. Mukhopadhyay, C. Bailey, A. Wander, B. Searle, C. Muryn, S. Schroeder, R. Lindsay, N. Weiher, and N. Harrison, Surf. Sci. **601**, 4433 (2007).
[110]N. Saito, C. Ishizaki, and K. Ishizaki, J. Ceram. Soc. Jpn. **102**, 301 (1994).
[111]F. Netzer and T. Madey, Surf. Sci. **127**, L102 (1983).
[112]J. Paul and F. Hoffman, J. Phys. Chem. **90**, 5321 (1986).
[113]U. Memmert, S. Bushby, and P. Norton, Surf. Sci. **219**, 327 (1989).
[114]H. Polzl, F. Zinka, D. Gleispach, and A. Winkler, Surf. Sci. **440**, 196 (1999).
[115]G. Tzvetkov, Y. Zubavichus, G. Koller, Th. Schmidt, C. Heske, E. Umbach, M. Grunze, M. Ramsey, and F. Netzer, Surf. Sci. **543**, 131 (2003).
[116]M. Schildbach and A. Hamza, Surf. Sci. **282**, 306 (1993).
[117]C. Nelson, J. Elam, M. Cameron, M. Tolbert, and S. George, Surf. Sci. **416**, 341 (1998).
[118]J. Elam, C. Nelson, M. Cameron, M. Tolbert, and S. George, J. Phys. Chem. B **102**, 7008 (1998).
[119]W. Mitchell, C. Chung, S. Yi, E. Hu, and W. Weinberg, Surf. Sci. **384**, 81 (1997).
[120]S. King, R. Davis, C. Ronning, and R. Nemanich, J. Electron. Mater. **28**, L34 (1999).
[121]S. King, R. Davis, and R. Nemanich, Surf. Sci. **602**, 405 (2008).
[122]R. Nemanich *et al.*, MRS Proc. **395**, 777 (1996).
[123]S. King, R. Nemanich, and R. Davis, J. Electrochem. Soc. **146**, 1910 (1999).
[124]S. King, E. Carlson, R. Therrien, J. Christman, R. Nemanich, and R. Davis, J. Appl. Phys. **86**, 5584 (1999).
[125]S. King, R. Nemanich, and R. Davis, J. Electrochem. Soc. **146**, 3448 (1999).
[126]S. King, R. Davis, and R. Nemanich, Surf. Sci. **603**, 3104 (2009).
[127]R. Culbertson, L. Feldman, and P. Silverman, J. Vac. Sci. Technol. **20**, 868 (1982).
[128]J. Craig, Jr., C. Cariss, and M. Craig, J. Vac. Sci. Technol., A **11**, 554 (1993).
[129]G. Ruano, J. Moreno-Lopez, M. Passeggi, Jr., R. Vidal, J. Ferron, M. Nino, R. Miranda, and J. de Miguel, Surf. Sci. **606**, 573 (2012).
[130]J. Miller, H. Siddiqui, S. Gates, J. Russell, Jr., J. Yates, Jr., J. Tully, and M. Cardillo, J. Chem. Phys. **87**, 6725 (1987).
[131]D. Parker, M. Jones, and B. Koel, Surf. Sci. **233**, 65 (1990).
[132]S. King, M. Benjamin, R. Nemanich, R. Davis, and W. Lambrecht, MRS Proc. **395**, 375 (1996).
[133]S. King, C. Ronning, R. Davis, R. Busby, and R. Nemanich, J. Appl. Phys. **84**, 6042 (1998).
[134]D. Briggs and M. Seah, *Practical Surface Analysis, Vol. 1—Auger and X-ray Photoelectron Spectroscopy* (Wiley, New York, 1990), p. 636.
[135]J. O'Hanlon, *A User's Guide to Vacuum Technology* (John Wiley & Sons, Hoboken, NJ, 2003), p. 492.
[136]T. Shirai, J. Wang, K. Matsumaru, C. Ishizaki, and K. Ishizaki, Sci. Technol. Adv. Mater. **6**, 123 (2005).
[137]O. Sneh, M. Cameron, and S. George, Surf. Sci. **364**, 61 (1996).
[138]O. Sneh and S. George, J. Phys. Chem. **99**, 4639 (1995).
[139]M. Flowers, N. Jonathan, A. Morris, and S. Wright, Surf. Sci. **351**, 87 (1996).
[140]K. Kawase, J. Tanimura, H. Kurokawa, K. Wakao, M. Inoue, H. Umeda, and A. Teramoto, J. Electrochem. Soc. **152**, G163 (2005).
[141]R. Shekhar and K. Jensen, Surf. Sci. **381**, L581 (1997).
[142]O. Ambacher, M. Brandt, R. Dimitrov, T. Metzger, M. Stutzman, R. Fischer, A. Miehr, A. Bergmaier, and G. Dollinger, J. Vac. Sci. Technol., A **14**, 3532 (1996).
[143]C. Chiang, S. Gates, A. Bensaoula, and J. Schultz, Chem. Phys. Lett. **246**, 275 (1995).
[144]U. Panyukova, H. Suzuki, R. Togashi, H. Murakami, Y. Kumagai, and A. Koukitu, Jpn. J. Appl. Phys., Part 2 **46**, L1114 (2007).
[145]Y. Kumagai, K. Akiyama, R. Togashi, H. Murakami, M. Takeuchi, T. Kinoshita, K. Takada, Y. Aoyagi, and A. Koukitu, J. Cryst. Growth **305**, 366 (2007).
[146]Z. Fan and N. Newman, Mater. Sci. Eng., B **87**, 244 (2001).
[147]K. Sinniah, M. Sherman, B. Lewis, W. Weinberg, J. Yates, Jr., and K. Janda, Phys. Rev. Lett. **62**, 567 (1989).